Journal of Alloys and Compounds 628 (2015) 325–328

Contents lists available at ScienceDirect

Journal of Alloys and Compounds

journal homepage: www.elsevier.com/locate/jalcom

Substitution of Ce for Nd in preparing $R_2Fe_{14}B$ nanocrystalline magnets

Z.B. Li [a,b], B.G. Shen [b,*], M. Zhang [b], F.X. Hu [b], J.R. Sun [b]

[a] Key Laboratory of Integrated Exploitation of Bayan Obo Multi-Metal Resources, Inner Mongolia University of Science and Technology, Baotou 014010, China
[b] State Key Laboratory for Magnetism, Institute of Physics, Chinese Academy of Sciences, Beijing 100190, China

ARTICLE INFO

Article history:
Received 8 July 2014
Received in revised form 6 December 2014
Accepted 8 December 2014
Available online 16 December 2014

Keywords:
Permanent magnets
$R_2Fe_{14}B$
Abundant element Ce
Magnetic properties

ABSTRACT

The substitution for Nd by abundant element Ce is a practical way for the comprehensive utilization of rare earth resources in permanent magnets. In this letter, we investigate the magnetic properties and magnetization reversal of $Nd_{12-x}Ce_xFe_{82}B_6$ ribbons by varying x from 0 to 12. These ribbons mainly consist of $R_2Fe_{14}B$ phase in isotropic nanostructure. Coercivity, Curie temperature and maximum energy product all decrease with the increase of Ce atomic percent. The decrease of coercivity is mainly attributed to the decrease of anisotropy due to the substitution for Nd by Ce. In $Ce_{12}Fe_{82}B_6$ and $Nd_1Ce_{11}Fe_{82}B_6$ ribbons, the magnetization reversal behaviors are more non-uniform and the squareness of demagnetization curve is poor in second quadrant. However, as long as the Ce concentration does not exceed 10 at.%, the squareness of demagnetization curve remains good and the intergranular exchange coupling is strong. It is expected that these investigations could be beneficial to the composition designing in the manufacturing of $R_2Fe_{14}B$ magnets.

1. Introduction

The finding of excellent magnetically hard properties in rare earth magnets of $(NdPr)_2Fe_{14}B$ has pushed for the technology development in many fields [1,2], and this type of materials is widely used in the areas of computer, energy, automotive industry, medical instruments, etc. However, Nd and Pr are less abundant in the natural rare earth resources. Since the rare earth mineral is paragenic ore, Ce element, also contained in the mineral, is the most abundant and low cost. Developing high abundant rare earth permanent magnets is necessary not only for cost reducing, but for integrated utilization of rare earth resource aiming to protect natural resources [3–9].

Recently, many works are focused on the substitution for Nd by using the abundant rare earth metals, such as Ce element [10–14], but the magnetic properties, especially the coercivity in $Ce_2Fe_{14}B$ are much inferior to those of $Nd_2Fe_{14}B$ and $Pr_2Fe_{14}B$ [8,10]. So developing $Ce_2Fe_{14}B$ magnets is a big challenge in science and technology. Actually, $Ce_2Fe_{14}B$ magnets process an anisotropy field of 26 kOe [10], much higher than that of hard ferrites magnets [15,16]. By additives method the maximum energy product of $(BH)_{max}$ = 28.2 MGOe were successfully achieved in the magnets with 40 wt% of Ce content in rare earth [17]. By the method of double main phases in preparing sintered magnets, the maximum energy product remains over 43 MGOe as the Ce content was 30% of the total amounts of all the rare earth metals [18]. So the partial substitution for Nd by Ce is a feasible way to improve the magnetic properties [19,20]. It is desirable to further improve the magnetic properties via optimizing the alloy composition and manufacturing process, and so it is necessary to investigate systematically and make it clearer about the phase constitution, structure and magnetic properties of $R_2Fe_{14}B$ by Ce substitution for Nd. Melt-spinning was used to obtain isotropic permanent magnets [21]. In this paper, we have prepared $Nd_{12-x}Ce_xFe_{82}B_6$ ribbons via melt-spinning method, and the behavior of magnetization reversal, the coercivity and Curie temperature are investigated with the variation of Ce content. It is expected that these investigations could be helpful for the composition designing in the manufacturing of rare earth magnets which contain high abundant rare earth Ce element.

2. Experimental

The precursor ingots $Nd_{12-x}Ce_xFe_{82}B_6$ were produced from the constituent elements by arc melting method under an argon atmosphere, and x (the atomic percent of Ce) varies from 0 to 12 (x = 0, 1, 2, 4, 6, 8, 10, 11, 12). Each ingot was remelted at least three times to ensure composition homogeneity. The precursor ingot was crushed into small pieces and inserted into a quartz tube, and then fixed the quartz tube in the chamber. The quartz tube has a bottom orifice whose diameter is in the range of 0.8–1.0 mm. The chamber was evacuated to a vacuum of 3×10^{-3} Pa followed by filled with high purity argon. The ribbons were obtained directly by induction melting the pieces and then ejecting the melt through the orifice onto the surface of a rotating copper wheel. The surface of copper wheel was

* Corresponding author. Tel.: +86 010 82648082.
E-mail address: shenbg@iphy.ac.cn (B.G. Shen).

http://dx.doi.org/10.1016/j.jallcom.2014.12.042
0925-8388/

polished using the 1000-grit paper, and the surface velocity of copper wheel was varied for optimizing the magnetic properties. The samples with optimum magnetic properties could be obtained with the surface velocity in the range of 20–25 m/s, except $Nd_1Ce_{11}Fe_{82}B_6$ and $Ce_{12}Fe_{82}B_6$ ribbons obtained with the optimum surface velocity of 27 m/s. The phase composition of the ribbons was examined by X-ray diffraction (XRD) using Cu Kα radiation, and cell was refined and the average grain size was estimated using Jade software. Magnetic measurements were performed using Lakeshore vibrating sample magnetometer (VSM) with the field direction in the plane of the ribbons and therefore the demagnetization factor was neglected.

3. Results and discussion

Fig. 1 shows the hysteresis loops of the optimally melt-spun ribbons at room temperature. With an increase of Ce atomic percent both the coercivity and saturation magnetization decrease. The magnetocrystalline anisotropy of $Ce_2Fe_{14}B$ is lower than that of $Nd_2Fe_{14}B$ [14], so the substitution by Ce decreases the magnetocrystalline anisotropy, which should be responsible for the decrease of coercivity. The decrease of saturation magnetization confirms that Ce ions possess smaller magnetic moments in $R_2Fe_{14}B$ magnets [10]. The variations of coercivity and energy product with Ce percent content are shown in the inset of Fig. 1. It is noted that in the magnets of $Ce_{12}Fe_{82}B_6$ and $Nd_1Ce_{11}Fe_{82}B_6$ with high content of Ce, the squareness of hysteresis loop is very poor, indicating more non-uniform and independent behaviors of magnetization reversal among grains in these two samples. The distribution of switch field could be used to check magnetization behavior and the squareness of hysteresis loop [22]. It can be seen in Fig. 2 that the main distribution of irreversible susceptibility (the distribution of irreversible susceptibility more than 0.2 times of the maximum one) is broader on the reduced field H/H_c in $Ce_{12}Fe_{82}B_6$ and $Nd_1Ce_{11}Fe_{82}B_6$ ribbons. Here H_c is the coercive field, and the distribution of x_{irr} is obtained from the recoil loops measured at room temperature. As the Ce content decreases and Nd content increases the main distribution of switch field becomes narrow, and the collectivity of magnetization behaviors and the squareness of hysteresis loop improve largely in $Nd_2Ce_{10}Fe_{82}B_6$ ribbons.

The magnetization behavior is sensitive to the structure, such as the grain size and phase composition which could be partially characterized by XRD. Fig. 3 shows XRD patterns for these optimally melt-spun ribbons. Based on the XRD patterns it confirms that all samples contain the isotropic $R_2Fe_{14}B$ structure phase, and that the average grain size are all in the range of 20–30 nm. The diffraction peaks are a little weak and broadened in $Ce_{12}Fe_{82}B_6$ and $Nd_1Ce_{11}Fe_{82}B_6$, indicating a smaller grains size in these two

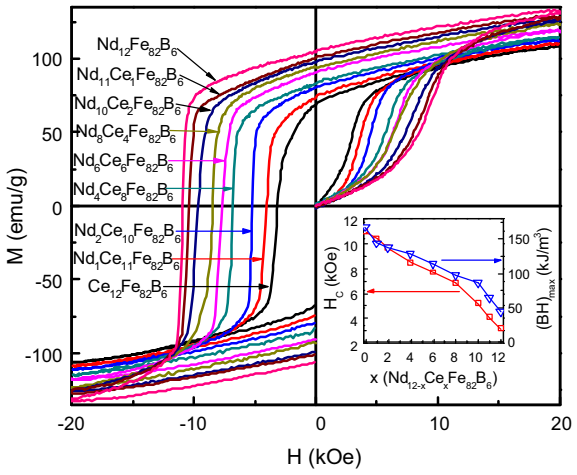

Fig. 1. The hysteresis loops for all samples of $Nd_{12-x}Ce_xFe_{82}B_6$ ribbons at room temperature. The inset shows the coercivity and maximum energy product with the variation of x from 0 to 12.

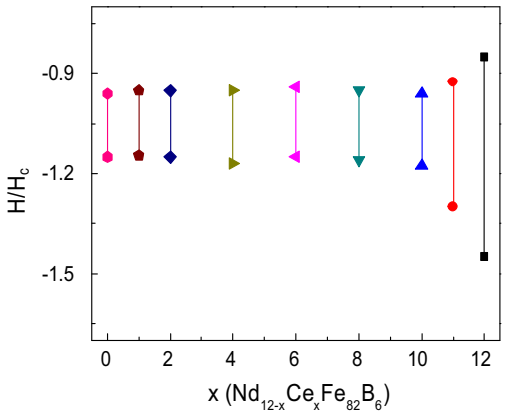

Fig. 2. The main distributions of irreversible susceptibility on the reduced field for all samples of $Nd_{12-x}Ce_xFe_{82}B_6$ ribbons.

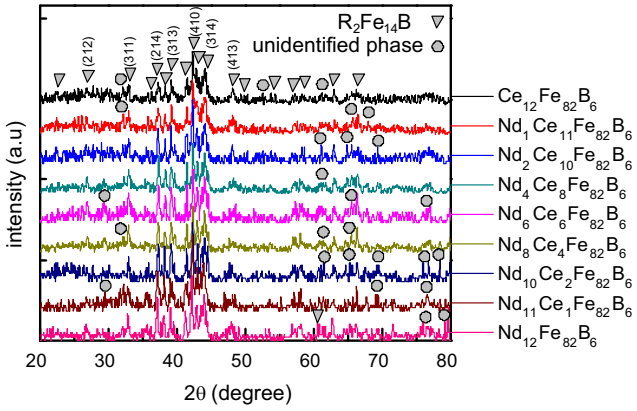

Fig. 3. XRD patterns for all samples of $Nd_{12-x}Ce_xFe_{82}B_6$ ribbons.

ribbons. It is noted that for a slow wheel velocity a larger grain size could be obtained in the $Ce_{12}Fe_{82}B_6$ and $Nd_1Ce_{11}Fe_{82}B_6$ ribbons, but the squareness of hysteresis loop deteriorates. It can be seen on the XRD patterns that the diffraction peaks are not very smooth and that besides the corresponding peaks of $R_2Fe_{14}B$ structure phase there are some weak peaks, indicating a little amount of metastable phases and amorphous phase at the intergranular interface in these ribbons. In $Ce_{12}Fe_{82}B_6$ and $Nd_1Ce_{11}Fe_{82}B_6$ ribbons, the fraction of metastable phase and amorphous phase is possibly slightly increased compared to the other samples reflecting the different phase equilibria in the Ce–Fe–B and Nd–Fe–B systems [14]. Both amorphous phase and metastable phase are probably weakly anisotropic and magnetically soft, which is assumed to be responsible for the deterioration in magnetic properties since the intergranular soft phase leads to a non-uniform magnetization reversal and a deterioration of hysteresis loop squareness [22]. In addition, with the increase of Ce content, most of diffraction peaks shift to a large angle, indicating a little decrease in lattice constant for the Ce substitution for Nd in $R_2Fe_{14}B$ magnets. The lattice constants are obtained by Jade software and listed in Table 1, and the coercivity and energy product are also listed in this table.

The magnetization reversal is strongly dependent on the intergranular exchange coupling. Henkel plots, which is defined as $\delta m = [2M_r(H) + M_d(H)]/M_r - 1$, could be used to check the exchange coupling between grains [23]. Here $M_r(H)$ is the remanence obtained after the application and subsequent removal of a field H in initial magnetization process, $M_d(H)$ is obtained after saturation in one direction and then the subsequent application and removal of a field H in the reverse direction, and M_r is the

Table 1
Lattice constant, coercivity and energy product of optimally melt-spun ribbons with $R_2Fe_{14}B$ structure.

Composition	Lattice constant a (nm)	Lattice constant c (nm)	H_c (kOe)	$(BH)_{max}$ (kJ/m^3)
$Nd_{12}Fe_{82}B_6$	8.81505	12.22604	10.935	167.63
$Nd_{11}Ce_1Fe_{82}B_6$	8.80518	12.21711	10.4	144.11
$Nd_{10}Ce_2Fe_{82}B_6$	8.80209	12.18264	9.61	137.92
$Nd_8Ce_4Fe_{82}B_6$	8.79613	12.18128	8.44	127.87
$Nd_6Ce_6Fe_{82}B_6$	8.79388	12.17983	7.68	114.57
$Ce_8Nd_4Fe_{82}B_6$	8.79294	12.17979	6.84	96.91
$Nd_2Ce_{10}Fe_{82}B_6$	8.78567	12.17959	5.18	86.43
$Nd_1Ce_{11}Fe_{82}B_6$	8.78555	12.16828	4.05	64.34
$Ce_{12}Fe_{82}B_6$	8.77919	12.15979	3.15	44.31

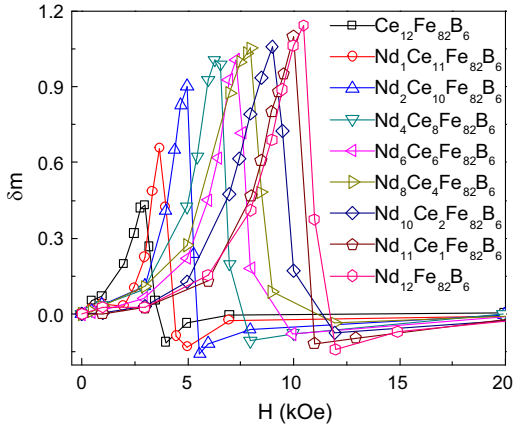

Fig. 4. δm curves (Henkel plots) for all samples of $Nd_{12-x}Ce_xFe_{82}B_6$ ribbons.

saturation remanence. Positive value of δm indicates that exchange coupling is dominant over the dipolar interaction. Fig. 4 shows δm values at room temperature for the optimally melt-spun samples, and the peak of δm on the curve is shown at the field around coercivity. In the $Ce_{12}Fe_{82}B_6$ and $Nd_1Ce_{11}Fe_{82}B_6$ ribbons, the maximum of δm is very low indicating a weak intergranular exchange coupling, which should partially results from the more amount of intergranular phase and be responsible for the poor squareness in the two samples [22].

Actually, besides the intergranular amorphous phase, the exchange coupling between grains should be dependent on the exchange constant at the interface that is related to the exchange constant in the main matrix [24]. The exchange constant could be evaluated by the Curie temperature [24], which is shown via magnetization versus temperature in Fig. 5. These curves were obtained in the following method. Firstly, magnetized the sample to saturation, and then increased the temperature and recorded the magnetization under the field at 1000 Oe. The red[1] arrow shows the abrupt decrease of magnetization to zero, which corresponds to Curie temperature. Curie temperature is controlled by 3d–3d and R–Fe exchanges [12]. It can be seen that with the increase of Ce atomic percent the Curie temperature decreases, indicating a smaller exchange constant between atoms in the unit cell since the low Curie temperature corresponds to low exchange energy against thermal perturbation. Even different with the results of Ref. [12] in the specific data, they are consistent in the variation trend. In $Ce_{12}Fe_{82}B_6$ and $Nd_1Ce_{11}Fe_{82}B_6$ ribbons, the Curie temperature is the lowest, indicating a small exchange constant, which is

[1] For interpretation of color in Fig. 5, the reader is referred to the web version of this article.

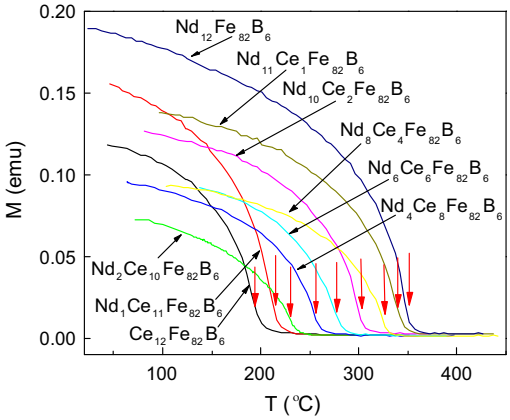

Fig. 5. Magnetization variations with temperature under the field of 1 kOe for all samples of $Nd_{12-x}Ce_xFe_{82}B_6$ ribbons.

possibly partially responsible for the weak intergranular exchange coupling effect and the poor squareness of hysteresis loop.

4. Conclusions

In summary, in $R_2Fe_{14}B$ magnets, with the increase of Ce content there is a slight decline in the lattice constant. The decrease of coercivity mainly results from the decrease of anisotropy in magnets due to the substation for Nd by Ce. The squareness of hysteresis loop deteriorates and the intergranular exchange coupling is weak in $Ce_{12}Fe_{82}B_6$ and $Nd_1Ce_{11}Fe_{82}B_6$ ribbons. But for the atomic percent of Ce less than 10%, the good squareness of hysteresis loop is mostly preserved without a significant weakening of the intergranular exchange coupling. The results of this investigation may serve as a reference for the research of ecologically and economically sustainable rare earth magnets.

Acknowledgements

The present work was supported by the National Basic Research Program of China (Grant No. 2014CB643702), and the National Natural Science Foundation of China (Grant No. 51461033).

References

[1] M. Sagawa, S. Fujimura, N. Togawa, H. Yamamoto, Y. Matsuura, J. Appl. Phys. 55 (1984) 2083.
[2] J.J. Croat, J.F. Herbst, R.W. Lee, F.E. Pinkerton, Appl. Phys. Lett. 44 (1984) 148.
[3] W. Gong, G.C. Hadjipanayis, J. Appl. Phys. 63 (1988) 3513.
[4] J. Yamasaki, H. Soeda, M. Yanagida, K. Mohri, N. Teshima, O. Kohmoto, T. Yoneyama, N. Yamaguchi, IEEE Trans. Magn. 22 (1986) 763.
[5] K.Y. Ko, S. Yoon, J.G. Booth, H.J. Al-Kanani, S.K. Cho, J. Mater. Sci. 37 (2002) 1421.
[6] K.Y. Ko, S. Yoon, J.G. Booth, J. Magn. Magn. Mater. 176 (1997) 313.
[7] I.I. Bulyk, V.V. Panasyuk, A.M. Trostianchyn, G.M. Grygorenko, Y.M. Pomarin, T.G. Taranova, V.A. Kostin, Y.G. Putilov, J. Alloys Comp. 370 (2004) 261.
[8] E. Niu, Z.A. Chen, G.A. Chen, Y.G. Zhao, J. Zhang, X.L. Rao, B.P. Hu, Z.X. Wang, J. Appl. Phys. 115 (2014) 113912.
[9] X.B. Liu, Z. Altounian, M. Huang, Q. Zhang, J.P. Liu, J. Alloys Comp. 549 (2013) 366.
[10] E. Burzo, Rep. Prog. Phys. 61 (1998) 1099.
[11] E.J. Skoug, M.S. Meyer, F.E. Pinkerton, M.M. Tessema, D. Haddad, J.F. Herbst, J. Alloys Comp. 574 (2013) 552.
[12] A. Alam, M. Khan, R.W. McCallum, D.D. Johnson, Appl. Phys. Lett. 102 (2013) 042402.
[13] M. Xing, J. Han, Z. Lin, F.M. Wan, C. Li, S. Liu, C. Wang, J. Yang, Y. Yang, J. Magn. Magn. Mater. 331 (2013) 140.
[14] J.F. Herbst, M.S. Meyer, F.E. Pinkerton, J. Appl. Phys. 111 (2012) 07A718.
[15] J.M.D. Coey, Scripta Mater. 67 (2012) 524.
[16] Z.M. Chen, B.R. Smith, B.M. Ma, J.W. Herchenroeder, Patent US7144463B2.
[17] S.X. Zhou, Y.G. Wang, R. Høier, J. Appl. Phys. 75 (1994) 6268.
[18] M. Zhu, W. Li, J. Wang, L. Zheng, Y. Li, K. Zhang, H. Feng, T. Liu, IEEE Trans. Magn. 50 (2014) 1000104.

[19] D. Li, Y. Bogatin, J. Appl. Phys. 69 (1991) 5515.
[20] L.H. Chu, Y. Liu, J. Li, Y.L. Ma, C.Y. Li, IEEE Trans. Magn. 48 (2012) 2092.
[21] Z. Chen, Y.Q. Wu, M.J. Kramer, B.R. Smith, B.M. Ma, M.Q. Huang, J. Magn. Magn. Mater. 268 (2004) 105.
[22] Z.B. Li, M. Zhang, B.G. Shen, J.R. Sun, Appl. Phys. Lett. 102 (2013) 102405.
[23] Z.B. Li, M. Zhang, L.C. Wang, B.G. Shen, X.F. Zhang, Y.F. Li, F.X. Hu, J.R. Sun, Appl. Phys. Lett. 104 (2014) 052406.
[24] H.W. Zhang, C.B. Rong, X.B. Du, S.Y. Zhang, B.G. Shen, J. Magn. Magn. Mater. 278 (2004) 127.